KINEMATICS, STATICS, AND DEXTERITY OF PLANAR ACTIVE STRUCTURE MODULES

Robert L. Williams II
Rex J. Kuriger
Ohio University
Athens, OH 45701

Automation in Construction
Vol. 7, 1997, pp. 77-89

Contact author information:
Robert L. Williams II
Assistant Professor
Department of Mechanical Engineering
257 Stocker Center
Ohio University
Athens, OH 45701-2979
Phone: (740) 593-1096
Fax: (740) 593-0476
E-mail: bobw@bobcat.ent.ohiou.edu

KINEMATICS, STATICS, AND DEXTERITY OF PLANAR ACTIVE STRUCTURE MODULES

Robert L. Williams II
Rex J. Kuriger
Ohio University
Athens, OH 45701

ABSTRACT

Construction automation could benefit from long-reach, lightweight, dexterous, strong, and stiff manipulators constructed from active structures (variable geometry trusses). Unfortunately, the few systems actually built to date have not delivered these desired characteristics (two such systems are heavy, slow, not dexterous enough, and too flexible) due to lack of unified, integrated, optimized design. This article presents a first step for integrated kinematic, static, dynamic, and control constraints in structural optimization. Workspace area, end-link angle, extension ratio, dexterity, and static loading are all considered in comparisons of basic planar active structure modules which could be used as joints in 3D active structures for construction automation.

1. INTRODUCTION

Active structures (also referred to as Variable Geometry Trusses) have great potential as a tool in construction automation. They are statically determinate trusses where some of the members are linear actuators, enabling the truss to articulate. The following are characteristics of active structures that represent potential improvements over the state-of-the-art in large serial manipulators. When properly designed, all active structure members are loaded axially, thus increasing stiffness and load bearing capability with a lightweight structure. They are modular, with kinematically redundant degrees-of-freedom (dof). The redundancy can be used to optimize performance, including snake-like motion to avoid obstacles. An active structure has an open structure allowing routing of cables hoses, and other utilities.

NASA originally developed the active structure concept for deployable space structures using 3D double octahedral modules [1]. This concept was later extended for active damping of deployable space structures [2] and use as a space crane [3]. A long-reach manipulator based on active structure modules has also been proposed for nuclear waste remediation [4,5]. Many authors have presented results for active structures, but the work has been almost exclusively in kinematics equations for Cartesian control of active structures [6-11]. Unfortunately, it appears NASA is no longer pursuing active structures for space due to smaller projects (although the Japanese Space Agency is still very much interested).

Active structures could be applied effectively for long-reach manipulators in construction automation on earth. However, due to gravity loading the design problem is more challenging than for space applications. Two different active structures realized in hardware for the 1G environment (PIPS at NASA Kennedy Space Center [12] and SERS for the DOE [13]) have not lived up to the promise of active structures because they are too heavy, too flexible, too slow, and not dexterous enough. One problem is complicated, offset joint design which decreases stiffness due to moment loading (ideally all

loads should be axial). In 3D active structure modules multiple independent spherical joints are required at the same point. Another major problem is the existing active structures have been designed in a traditional serial fashion (kinematics then structures then controls).

The current authors contend that active structures are viable candidates for construction automation in 1G. This article presents a first step in integrated design optimization for active structures. The kinematics, dynamics, structural, and controls design must be considered in an integrated manner if lightweight, dexterous, compact, stiff active structure manipulators are to be achieved. This article focuses on 2D active truss modules (2D and 3D active structure modules are surveyed in [14]) used for joints in construction robots. Planar joints require only revolute joints so it is easier to design the overall manipulator members for axial loading only. 3D motion can be obtained by combining planar modules in perpendicular planes and/or using conventional rotary joints along the active structure.

This article considers kinematics, dynamics, workspace, dexterity, compactness, and static strut loading for two basic planar active structure module designs: the batten-actuated truss (BAT) and the longeron-actuated truss (LAT). All of these factors must be considered concomitantly because most are competing factors and there are tradeoffs in design. Standard structural optimization techniques may be applied for overall manipulator design using these various factors as constraints, but the problem is compounded due to the infinite configurations for active structures. Using the results of this article, this structural optimization can be pursued to produce viable construction automation manipulators.

2. BASIC MODULE CHARACTERISTICS

Figures 1 shows two basic choices for planar active structure articulation and resisting an externally-applied vertical load F_E (the batten-actuated truss, BAT and the longeron-actuated truss, LAT). L_V and L_0 are fixed length members and L_i is a variable length which is varied to control the angle θ_i (which gives the angle of link L_V from the horizontal. Another active module was considered, a modified LAT, where L_V is also variable. This module presented good range of motion but at the cost of an extra actuator and the possibility of active structures which fold through themselves. Therefore, the focus of this article is the BAT and LAT modules. The results in this section have $L_0 = 1$, $L_V = \sqrt{2}$, and $\sqrt{2} - 1 \le L_i \le \sqrt{2} + 1$.

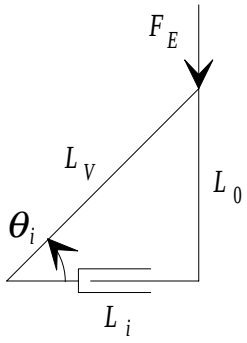

Figure 1a. BAT Actuation

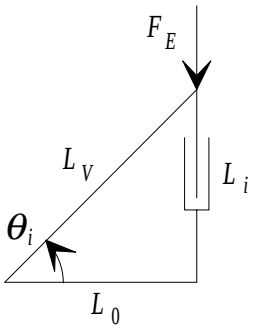

Figure 1b. LAT Actuation

These basic alternatives have different kinematic and static characteristics. From the law of cosines, the θ_i vs. L_i relationship can be expressed for each case:

$$\theta_{i_{BAT}} = \cos^{-1}\left[\frac{L_V^2 + L_i^2 - L_0^2}{2L_V L_i}\right] \qquad \theta_{i_{LAT}} = \cos^{-1}\left[\frac{L_V^2 + L_0^2 - L_i^2}{2L_V L_0}\right] \tag{1}$$

Figure 2a shows that θ_i for the BAT is very sensitive to changes in L_i; also, the maximum angle θ_i is only 45° because the angle decreases back to zero after L_i passes through 1.0. If the full limits on L_i are allowed, both modules start and end with all members folded on the horizontal axis. The LAT angle kinematics are much preferable: the range is much larger (theoretically 180°) and the slope is nearly linear in most of the range, as seen in Fig. 2b. For practical active structures, tighter limits than $\sqrt{2}-1 \le L_i \le \sqrt{2}+1$ must be imposed. The static force characteristics of Figs. 3a and 3b are similar: high breakaway actuator forces required when the modules are folded up. Both have reasonable actuator forces (F_i, axial force required on active strut) in the useful motion range. However, the maximum angle range for the BAT is much more constrained than the LAT case (45° vs. 180°). Standard SI units are used throughout this article: *m* for length, *N* for force; all angles are in *degrees*.

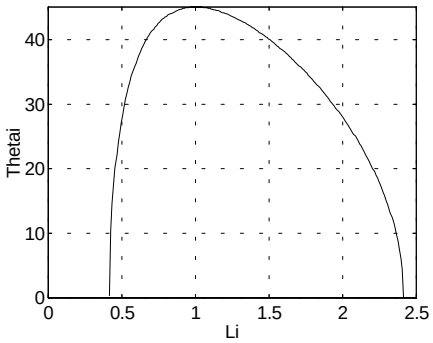

Figure 2a. BAT Angle θ_i vs. L_i

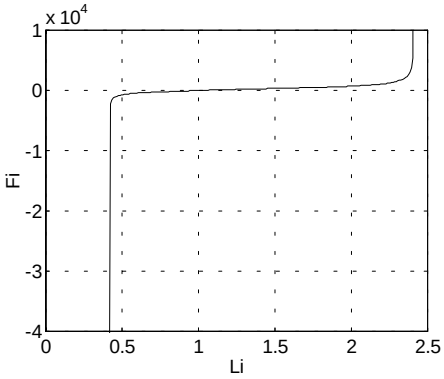

Figure 2b. BAT Actuator Force F_i vs. L_i

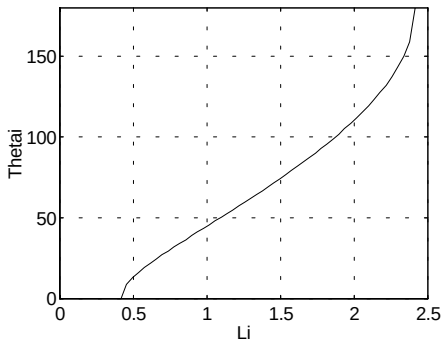

Figure 3a. LAT Angle θ_i vs. L_i

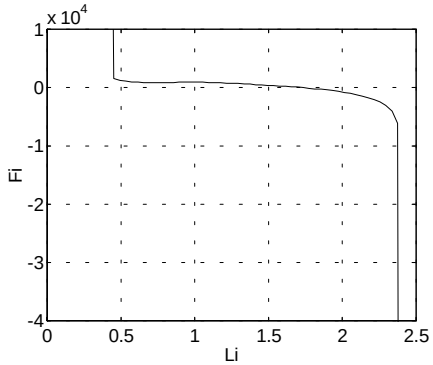

Figure 3b. LAT Actuator Force F_i vs. L_i

3. PLANAR ACTIVE STRUCTURE CHARACTERISTICS

The basic planar actuation schemes from the section above were combined to form basic planar active structure joint modules: the three degree-of-freedom (dof) BAT and the four-dof LAT. The purpose of this section is compare the workspace, static loading, dexterity, and extension ratios of these basic modules which can be used as joints in active structure manipulators for construction automation. Figures 4 and 5 show four joints considered, the BAT and LAT with different fixed length relationships, $L_V = \sqrt{2}L_0$ and then $L_V = L_0$. For all cases, the joint limits were arbitrarily set to $0.45L_0 \le L_i \le L_0$ for comparison.

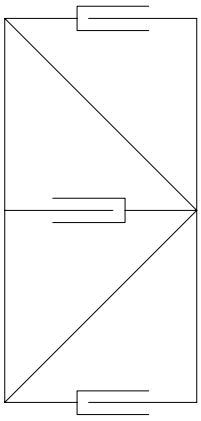

Figure 4a. BAT Module, $L_V = \sqrt{2}L_0$

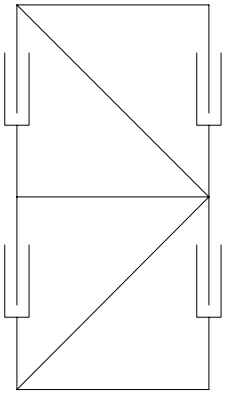

Figure 4b. LAT Module, $L_V = \sqrt{2}L_0$

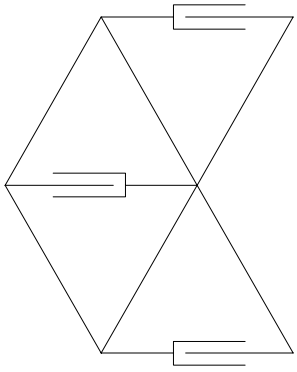

Figure 5a. BAT Module, $L_V = L_0$

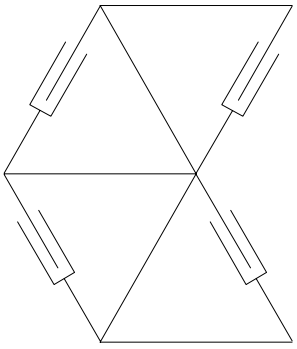

Figure 5b. LAT Module, $L_V = L_0$

3.1 Workspace

This section presents a comparison of the planar reachable workspace area for the above four active structure joints. Workspace determination for serial manipulators is well understood (e.g. [15]). Workspace determination is not as straight-forward for parallel manipulators. In this section the planar workspace areas for the modules of Figs. 4 and 5 are determined by the appropriate combinations of minimum and maximum actuator joint limits to trace the workspace boundary. The *x*,*y* reachable workspaces are shown in the figures below. Dexterous workspace is defined as that area reachable for all end-link orientations; this is generally null for active structures. Attached to the workspace boundaries below is an indication of end-link angle. For each case, the horizontal end-link workspace is a central vertical straight line (not shown).

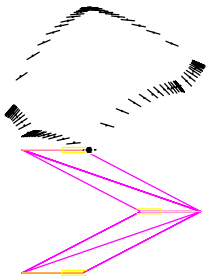

Figure 6a. BAT Workspace, $L_V = \sqrt{2}L_0$

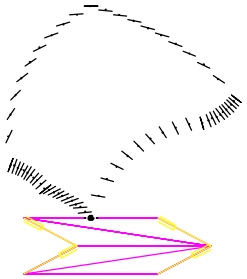

Figure 6b. LAT Workspace, $L_V = \sqrt{2}L_0$

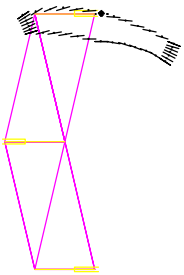

Figure 7a. BAT Workspace, $L_V = L_0$

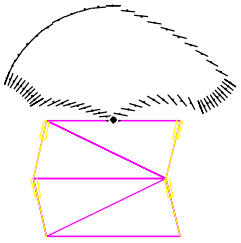

Figure 7b. LAT Workspace, $L_V = L_0$

Table 1 summarizes the workspace areas (with $L_0 = 1$) for the four cases, the end-link angle ranges, and the unitless extension ratios (defined as the maximum extended height divided by the minimum). For this comparison, the LAT $L_V = \sqrt{2}L_0$ is superior.

	Area (m^2)	**Angle** (*deg*)	**Extension Ratio**
BAT $L_V = \sqrt{2}L_0$	0.65	±57	2.20
LAT $L_V = \sqrt{2}L_0$	1.47	±73	4.80
BAT $L_V = L_0$	0.20	±34	1.25
LAT $L_V = L_0$	0.90	±68	1.97

Table 1. Workspace and Extension Ratio Results

3.2 Statics

For the same four active structure joint cases from above, this section presents the static loading on each member as the structure articulates through its workspace. Closed-form equations were derived from the static equilibrium requirement for each case. It was discovered that the worst-case loading member loading was encountered on the workspace boundary. Figure 8 shows the BAT static loading model including link numbering, where a downward negative force of F_E = 500 *N* is externally applied to each end-link node (the LAT model is similar). For this loading case, Figs. 9 (*BAT* $L_V = \sqrt{2}L_0$) and Figs. 10 (*LAT* $L_V = \sqrt{2}L_0$) show static axial force results for each of the nine links. Each plot has the same scale and shows the tension/compression loading on each member as the workspace boundary is traced (the independent variable for each plot is the *x* coordinate of the workspace). Table 2 summarizes the maximum loads (+tension/-compression) and average loading for each member around the workspace boundary (ave.) for the BAT and LAT cases. Again, the LAT $L_V = \sqrt{2}L_0$ is superior for

static loading. The *BAT* $L_V = L_0$ and *LAT* $L_V = L_0$ cases are not shown due to space constraints; both of these cases experience less severe static loading than the two cases shown.

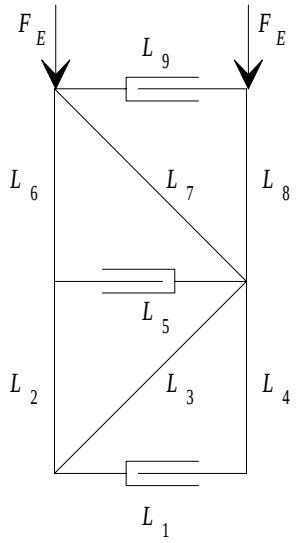

Figure 8. BAT Static Axial Forces Model

Link	1	2	3	4	5	6	7	8	9
BAT	-5619	-5772	6009	-6341	-10230	-5772	6778	-1079	-1078
Ave.	-1551	-2402	3575	-1844	-3836	-2402	2378	-614	-331
LAT	-3043	-2378	2961	-3435	-4215	-2378	3051	-1079	-1079
Ave.	-896	-986	1494	-1154	-1491	-986	1010	-550	-308

Table 2. BAT and LAT ($L_V = \sqrt{2}L_0$) *Static Axial Forces (N) Analysis Summary*

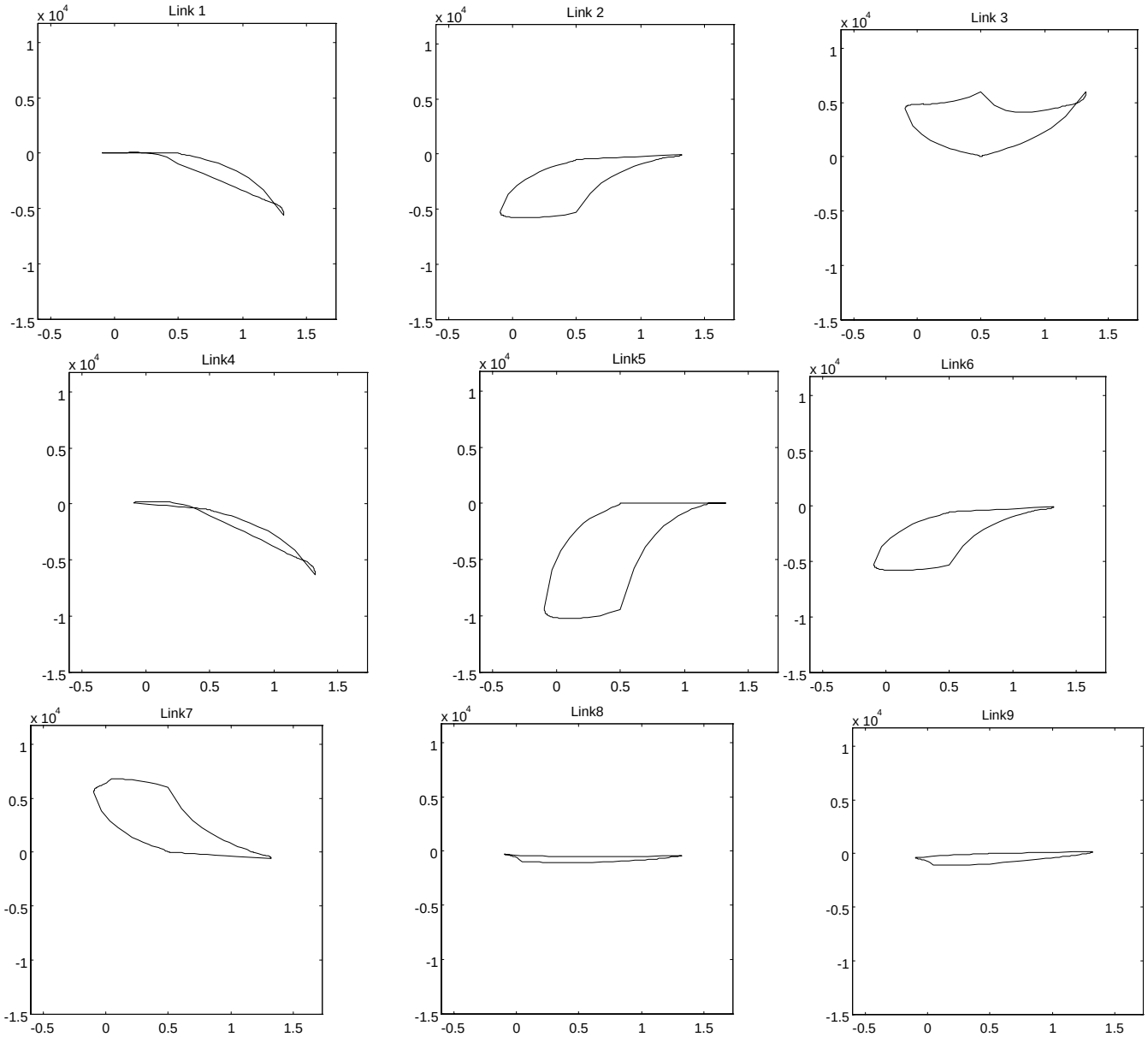

Figure 9. BAT Axial Forces (N) Results, $L_V = \sqrt{2}L_0$

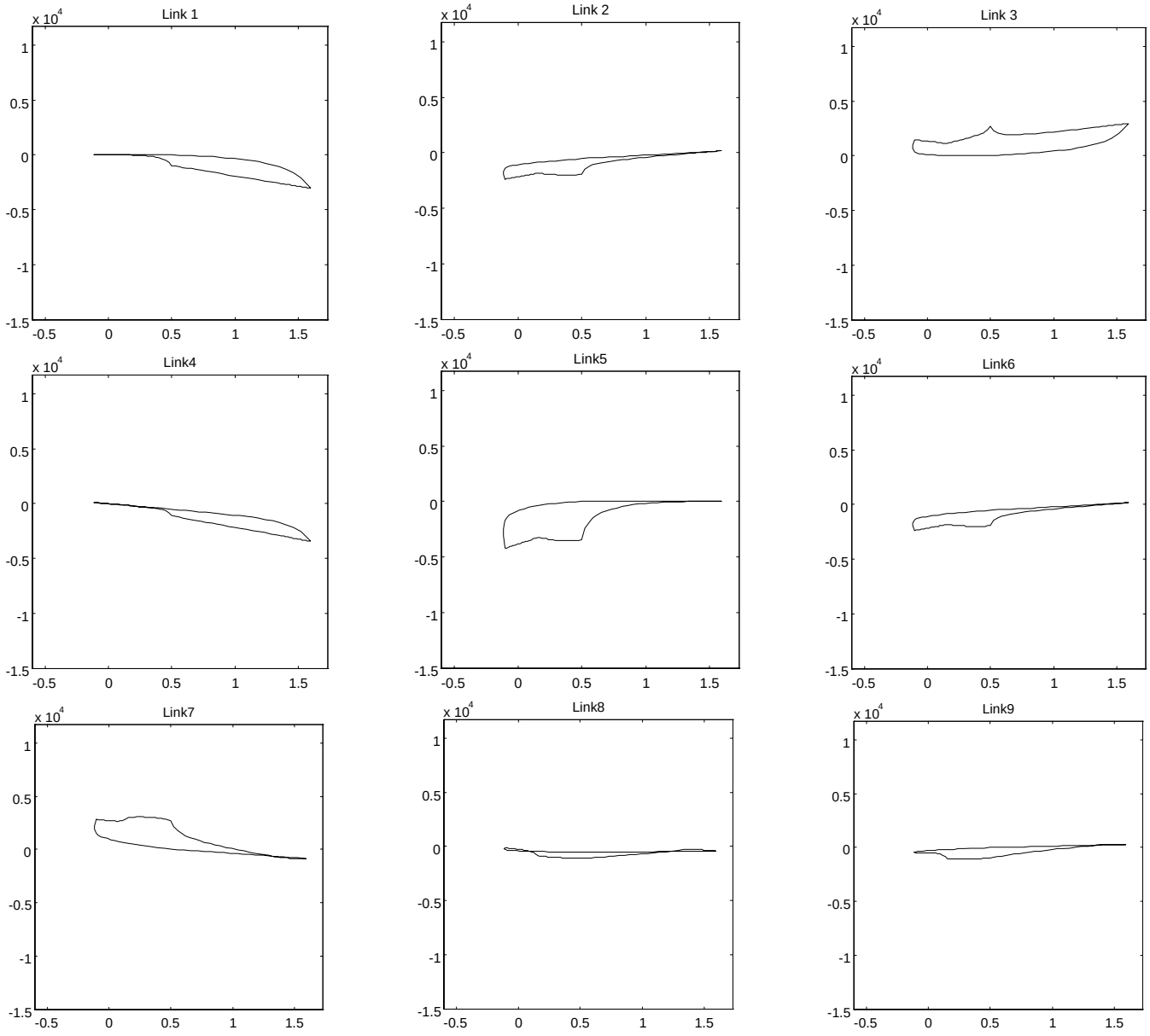

Figure 10. LAT Axial Forces (N) Results, $L_V = \sqrt{2}L_0$

3.3 Dexterity

In addition to workspace characteristics and static loading, dexterity was considered for the four active structure joints under comparison. Yoshikawa [18] proposes the manipulability index $\sqrt{JJ^T}$ to represent dexterity, where J is the manipulator Jacobian matrix. Klein and Blaho [19] compare various measures of dexterity for kinematically-redundant manipulators, including the manipulability index.

Dexterity for active structures is important because dexterity measures give an indication of how close the active structure is to a kinematic singularity, where freedom to move in one or more Cartesian directions is lost. For example, $\sqrt{JJ^T} = 0$ at a kinematically-singular configuration, and so we wish to maximize the manipulability index to avoid singularities. Due to the duality of velocity and force, static structural loading is improved at singular configurations because large loads may be resisted with small actuator forces (the load is largely taken by rigid members). Therefore, while active structure singularities are bad for Cartesian motion, they are generally good for static loading.

In this article, the dexterity measures considered are the manipulability index and the minimum singular value for the module Jacobian matrix J (where J maps linear actuator rates $\dot{L}$ to Cartesian rates $\dot{X} = J\dot{L}$). For 3-dof planar Cartesian motions, there are three singular values for each Jacobian matrix, but only the minimum is compared to give the worst-case scenario in the second dexterity measure. If either dexterity measure is zero, the active structure module is in a singular configuration and has lost a degree of freedom. Higher values correspond to greater dexterity.

It was found that none of the four modules of Figs. 4 and 5 is ever singular (both dexterity measures are always greater than zero over the entire translational and rotational workspace in each case). The BAT $L_V = \sqrt{2}L_0$ case was found to have the highest dexterity, but this corresponds to a much smaller workspace than the LAT $L_V = \sqrt{2}L_0$ case. Therefore, in this article, good dexterity is defined as

singularity-free modules; all four modules meet this criterion and so dexterity is not a major module design factor. Further work is required in this area because when singularity-free (by virtue of joint limits) planar modules are combined into general 3D active structures, kinematic singularities may result.

3.4 BAT Sensitivity

This concludes the basic comparison of the four cases. However, two more cases are presented to investigate different joint limit effects. In this section, BAT sensitivity is demonstrated by increasing the actuating range of the variable members to $0.415L_0 \le L_i \le L_0$ (from $0.45L_0 \le L_i \le L_0$). Such a small change makes a large difference because this is the steep range on the θ_i vs. L_i curve of Fig. 2a. Figure 11 and Table 3 show an amazing increase in workspace area and extension ratio due to this small actuator limit change. However, Table 4 shows the cost of this increased kinematic performance: the static loading becomes extremely high in the compact configurations because the largely horizontal actuato

Figure 11. BAT Workspace
$0.45L_0 \le L_i \le L_0$ (left) and $0.415L_0 \le L_i \le L_0$ (right)

	Area (m^2)	**Angle** (*deg*)	**Extension Ratio**
$0.45L_0 \le L_i \le L_0$	0.65	±57	2.2
$0.415L_0 \le L_i \le L_0$	1.73	±84	13.7

Table 3. BAT Sensitivity Characteristics

Link	1	2	3	4	5	6	7	8	9
Max.	-56178	-39676	56053	-56329	-79139	-39676	46446	-6833	-6815
Ave.	-15122	-12231	27028	-15319	-24067	-12231	134.8	-1600	-1393

Table 4. BAT $0.415L_0 \le L_i \le L_0$ *Static Axial Forces (N) Analysis Summary*

If large extension ratios are required, it is possible to use passive springs to unload actuators in folded configuration. However, the BAT sensitivity and limited θ_i range are detriments to this module.

3.5 LAT Hydraulic Limits

The second additional analysis evaluates the LAT with an actuating range of $0.75L_0 \le L_i \le 1.25L_0$ which matches nominal hydraulic actuator joint limits (likely required for operations in 1G). Figure 12 and Table 5 show a decrease in kinematic performance (smaller workspace and extension ratio) for this case, but the associated static loading in Table 6 is reduced, both compared to the arbitrary $0.45L_0 \le L_i \le L_0$ limits in the above sections.

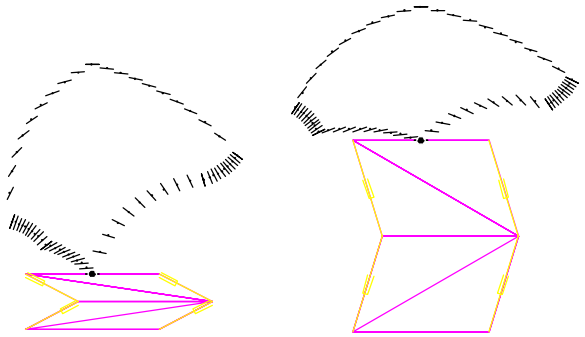

Figure 12. LAT Workspace
$0.45L_0 \le L_i \le L_0$ (left) and $0.75L_0 \le L_i \le 1.25L_0$ (right)

	Area (m^2)	**Angle** (*deg*)	**Extension ratio**
$0.45L_0 \le L_i \le L_0$	1.47	±73	4.8
$0.75L_0 \le L_i \le 1.25L_0$	1.25	±58	1.7

Table 5. LAT Joint-Limit Characteristics

Link	**1**	**2**	**3**	**4**	**5**	**6**	**7**	**8**	**9**
Max.	-493	-1200	442	-1691	-700	-1200	1062	-523	-376
Ave.	-158	-435	49	-575	-261	-435	38	-430	-13

Table 6. LAT $0.75L_0 \le L_i \le 1.25L_0$ *Static Axial Forces (N) Analysis Summary*

4. CARTESIAN CONTROL OF ACTIVE STRUCTURES

As mentioned in the introduction, coordination of the various active structure actuator lengths to achieve commanded Cartesian motions has been the focus of most prior efforts in this field (e.g. [6-11]). This section presents a Cartesian control method similar to Salerno's approach [6], adapted from conventional Cartesian control of kinematically-redundant serial manipulators. The general method is rate-based local optimization and was first presented by Liegois [16]. For an excellent overview of this topic with numerous references, please see [17].

As mentioned in Section 3.3, the active structure Jacobian matrix J maps n-dimensional linear actuator rates $\dot{L}$ to m-dimensional Cartesian rates: $\dot{X} = J\dot{L}$. If $n>m$, the active structure is kinematically-redundant. The basic equation for Cartesian trajectory following and performance optimization is [16]:

$$\dot{L} = J^{+}\dot{X} + \left(I - J^{+}J\right)z \tag{2}$$

where $J^{+} = J^{T}\left(JJ^{T}\right)^{-1}$ is the Moore-Penrose pseudoinverse of the rectangular Jacobian matrix, $\left(I - J^{+}J\right)$ is the null-space projection matrix, and z is a vector chosen to optimize a performance objective (obstacle avoidance, joint limit avoidance, and singularity avoidance, among others [17]). If the active structure is in the neighborhood of a kinematic singularity, a singularity-robust singular value decomposition (SVD) method may replace the Moore-Penrose pseudoinverse. Cartesian tracking error will result in singular neighborhoods, but the SVD algorithm yields bounded results.

Figure 13 presents the block diagram for controlling an active structure using this Cartesian method. The commanded Cartesian velocity $\dot{X}$ for the active structure endpoint frame and the

performance optimization vector *z* are inputs. The resulting actuator length rates $\dot{L}$ are integrated to actuator lengths *L* commanded to the active structure and achieved via linearized independent PID servo controllers (L_{actual} is the vector of currently-sensed actuator lengths).

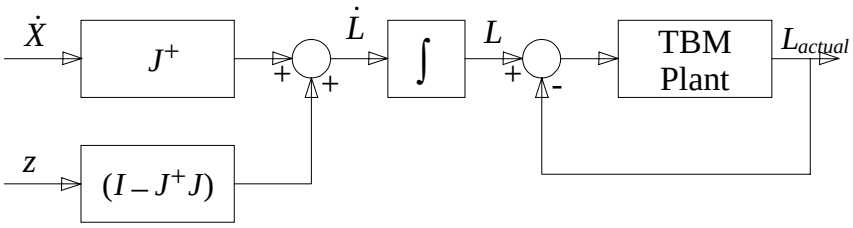

Figure 13. Cartesian Controller for Active Structures

This method applies to any general spatial active structure. It can handle 3D active structures composed of 3D joints or 2D joints such as the BAT and LAT compared in this article. For instance, Fig. 14 shows a spatial active structure comprised of two planar BAT (or LAT, depending on where the linear actuators are placed) joints, connected in perpendicular planes and separated by a static truss module.

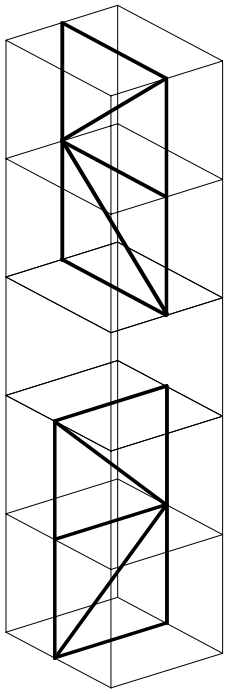

Figure 14. Spatial Active Structure Composed of Planar Joints

A Cartesian control algorithm (the Virtual Serial Manipulator Control method) with potential benefits over the method in this section has been developed and is presented in [11]. The basic idea is to replace the complexity of the in-parallel-actuated modules with relatively simpler, kinematically-equivalent, virtual serial manipulator chains. This method has been successfully applied to control of spatial DOE active structure hardware [13]. Details are beyond the scope of the current article.

5. CONCLUSION

Active structures (variable geometry trusses) have great potential as long-reach, lightweight, strong and stiff manipulators for construction automation. However, two active structure hardware systems developed for 1G applications have not delivered these desirable characteristics due to lack of integrated, optimized design. For success, the designs must admit kinematic, dynamic, static, and control constraints simultaneously rather than in a traditional serial fashion. Figure 15 shows an integrated, iterative design flow for active structures which will be pursued using the results of this article.

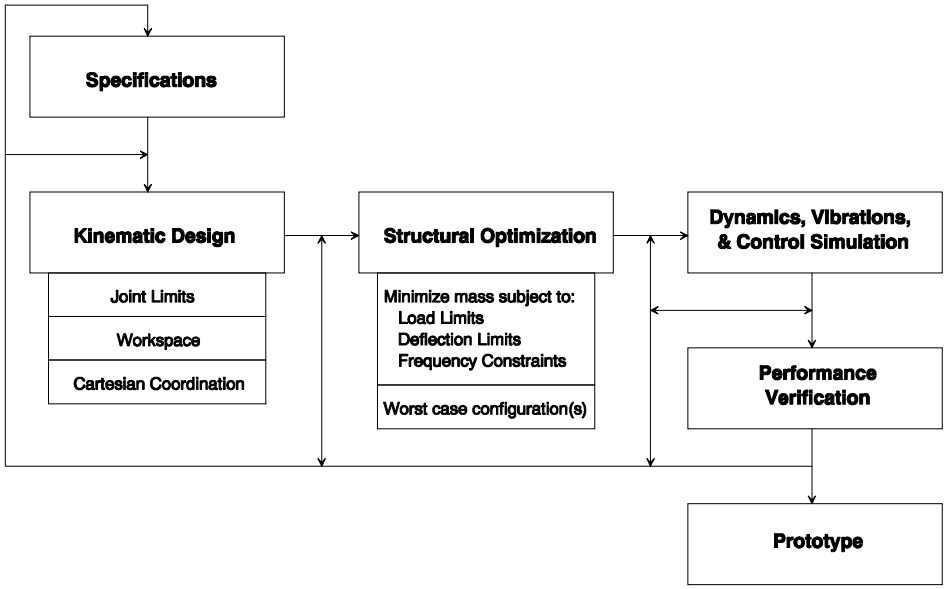

Figure 15. Integrated Active Structure Design Flow

Proposed 3D active structure modules work fine in theory but experience a large stiffness knockdown in practical implementations, due to difficulty of constructing multiple independent passive spherical joints at the same point. Previous works in active structures have focused almost exclusively on coordinating the desired Cartesian motion with the many linear actuators. This article has focused on

two basic planar active structure joint designs, the BAT and LAT modules. 3D articulating structures may be formed by combining these joints in perpendicular planes.

The primary contribution of this article is consideration of workspace, extension ratio, dexterity, and static loading in comparison of different planar joint designs. Dynamics equations have been developed (but not reported here), for the Section 2 modules. Dynamics simulation was found to exacerbate the high breakaway forces required in the static actuator force plots of Figs. 2b and 3b. In addition, a Cartesian control algorithm has been described, which should be considered during the active structure design process rather than afterwards.

The BAT module is attractive at first due to high extension ratio. However, both high sensitivity of θ_i to small changes in L_i and small θ_i range tend to make this candidate unsuitable for 1G operations (unless passive springs can be employed to alleviate the extremely high actuator forces required). The LAT module ($L_V = \sqrt{2}L_0$ case) was the clear choice in terms of the competing factors considered: workspace area and end-link angle, extension ratio, dexterity, and static member loading. Among these factors, dexterity was found to be least important since all modules avoid singularities throughout their workspaces. However, dexterity will be a crucial issue in future work with 3D active structures composed of 2D modules. All these factors (plus dynamics and control algorithms) must be considered simultaneously for effective active structures optimization.

6. REFERENCES

[1] M.D. Rhodes and M.M. Mikulas Jr., 1985, "*Deployable Controllable Geometry Truss Beam*", NASA Technical Memorandum 86366.

[2] R.H. Wynn, and H.H. Robertshaw, 1991, "*The Control of Flexible Structure Vibrations Using a Cantilevered Adaptive Truss*", Proceedings of the AIAA/ASME/ASCE/ASC 32nd Structures, Structural Dynamics, and Materials Conference, DE-Vol. 26, Baltimore, MD, pp. 2190-2196.

[3] G.S. Chen and B.K. Wada, 1990, "*On an Adaptive Truss Manipulator Space Crane Concept*", 1st Joint US/Japan Conference on Adaptive Structures, Maui, Hawaii.

[4] R.J. Salerno and C.F. Reinholtz, 1994, "*A Modular, Long-Reach, Truss-Type Manipulator for Waste Storage Tank Remediation*", Proceedings of the 1994 ASME Mechanisms Conference, DE-Vol. 72, Minneapolis, MN, September, pp. 153-159.

[5] R.S. Stoughton, J.C. Tucker, and C.G. Horner, 1995, "*A Variable Geometry Truss Manipulator for Positioning Large Payloads*", Proceedings of the ANS Sixth Topical Meeting on Robotics and Remote Systems, Monterey, CA, February**,** pp. 239-244.

[6] R.J. Salerno, 1993, "*Positional Control Strategies for a Modular, Long-Reach, Truss-Type Manipulator*", Ph.D. Dissertation, Virginia Polytechnic Institute & State University.

[7] G.S. Chirikjian and J.W. Burdick, 1991, "*Parallel Formulation of the Inverse Kinematics of Modular Hyper-Redundant Manipulators*", Proceedings of the 1991 IEEE International Conference on Robotics and Automation, Sacramento, CA.

[8] F. Naccarato, and P.C. Hughes, 1991, "*Inverse Kinematics of Variable-Geometry Truss Manipulators*", Journal of Robotic Systems, 8(2): 249-266.

[9] M. Subramaniam and S.N. Kramer, 1992, "*The Inverse Kinematic Solution of the Tetrahedron Based Variable-Geometry Truss Manipulator*", Journal of Mechanical Design, 114: 433-437.

[10] B. Padmanabhan, V. Arun, and C.F. Reinholtz, 1992, "*Closed-Form Inverse Kinematic Analysis of Variable-Geometry Truss Manipulators*", Journal of Mechanical Design, 114.

[11] R.L. Williams II and J.B. Mayhew IV, 1995, "*Coordination of Modular Truss-Based Manipulators: The Virtual Serial Manipulator Approach*", submitted to the Journal of Mechanical Design.

[12] R.L. Williams II, 1996, "*Follow-the-Leader Control for the Payload Inspection and Processing System Prototype Hardware*", Final Report, NASA/ASEE Summer Faculty Fellowship Program, NASA Kennedy Space Center.

[13] R.L. Williams II, J.B. Mayhew IV, and J.C. Tucker, 1997, "*Cartesian Control of Truss-Based Manipulators"*, Proceedings of the American Nuclear Society Seventh Topical Meeting on Robotics and Remote Systems, Augusta, GA.

[14] R.L. Williams II, 1995, "*Survey of Active Truss Modules*", ASME Design Technical Conferences, Boston, MA.

[15] K.C. Gupta, 1986, "*On the Nature of Robot Workspace*", International Journal of Robotics Research, 5(2): 112-121.

[16] A. Liegeois, 1977, "*Automatic Supervisory Control of the Configuration and Behavior of Multibody Mechanisms*", IEEE Transactions on SMC, 17(12): 868-871.

[17] D.N. Nenchev, 1989, "*Redundancy Resolution Through Local Optimization: A Review*", Journal of Robotic Systems, 6(6): 769-798.

[18] T. Yoshikawa, 1985, "*Manipulability of Robotic Mechanisms*", International Journal of Robotics Research, 4(2): 3-9.

[19] C.A. Klein and B.E. Blaho, 1987, "*Dexterity Measures for the Design and Control of Kinematically Redundant Manipulators*", International Jnl of Robotics Research, 6(2): 72-83.